JAIST Repository
https://dspace.jaist.ac.jp/

Title	Investigation into Structural Phase Transitions in Layered Titanium-Oxypnictides by a Computational Phonon Analysis
Author(s)	Nakano, Kousuke; Hongo, Kenta; Maezono, Ryo
Citation	Inorganic Chemistry, 56(22): 13732-13740
Issue Date	2017-11-02
Type	Journal Article
Text version	publisher
URL	http://hdl.handle.net/10119/15356
Rights	This is an open access article published under an ACS AuthorChoice License (http://pubs.acs.org/page/policy/authorchoice_termsofuse.html), which permits copying and redistribution of the article or any adaptations for non-commercial purposes. Kousuke Nakano, Kenta Hongo, and Ryo Maezono, Inorganic Chemistry, 56(22), 2017, 13732-13740. DOI:10.1021/acs.inorgchem.7b01709
Description	

JAIST
JAPAN
ADVANCED INSTITUTE OF
SCIENCE AND TECHNOLOGY

Japan Advanced Institute of Science and Technology

This is an open access article published under an ACS AuthorChoice License, which permits copying and redistribution of the article or any adaptations for non-commercial purposes.

Inorganic Chemistry

Article

Cite This: Inorg. Chem. 2017, 56, 13732-13740

pubs.acs.org/IC

Investigation into Structural Phase Transitions in Layered Titanium-Oxypnictides by a Computational Phonon Analysis

Kousuke Nakano,*[,⊥] Kenta Hongo,[†,‡,§] and Ryo Maezono*[,⊥]

[†]Research Center for Advanced Computing Infrastructure, JAIST, Asahidai 1-1, Nomi, Ishikawa 923-1292, Japan

[‡]PRESTO, Japan Science and Technology Agency (JST), Kawaguchi, Saitama 332-0012, Japan

[§]Center for Materials Research by Information Integration, Research and Services Division of Materials Data and Integrated System, National Institute for Materials Science, Tsukuba 305-0047, Japan

[⊥]School of Information Science, JAIST, Asahidai 1-1, Nomi, Ishikawa 923-1292, Japan

ABSTRACT: We applied *ab initio* phonon analysis to layered titanium-oxypnictides, $Na_2Ti_2Pn_2O$ (Pn = As and Sb), and found a clear contrast between the cases with lighter/heavier pnictogen in comparison with experiments. The result completely explains the experimental structure at low temperature, $C2/m$ for Pn = As, within the conventional charge density wave, while there arise discrepancies when the pnictogen gets heavier. Our phonon calculation using the GGA-PBE functional predicts that a *Cmce* polymorph is more stable than the experimentally observed one (*Cmcm*) for Pn = Sb. On the basis of further quantitative analysis, we suggest the possibility that the GGA-PBE functional does not properly reproduce the electron correlation effects for Pn = Sb, and this could be the reason for the present discrepancy.

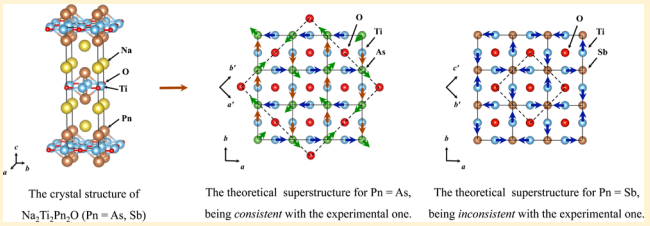

INTRODUCTION

Recently discovered layered titanium-oxypnictides, ATi_2Pn_2O [A = Na_2, Ba, $(SrF)_2$, and $(SmO)_2$; Pn = As, Sb, and Bi],[1−13] comprise a new superconducting family, and this superconducting mechanism has attracted intensive attentions because the crystal and electronic structures are similar to those of exotic superconductors such as cuprates[14] or iron arsenides.[15] The superconducting mechanism has been expected to be electron−phonon driven,[16−19] and the accompanying singularities in resistivity and susceptibility at low temperature are regarded as being due to conventional charge density wave (CDW).[17,19−21] Though our latest phonon evaluation using GGA-PBE without assuming any magnetic orderings revealed that the singularities could be explained within the conventional CDW for Pn = As,[22] it is still unknown if this is the case for Pn = Sb and Bi.[16,22] Interestingly, recent works are pointing out the possibility of exotic mechanism of the structural transition for these compounds: For $BaTi_2Pn_2O$ (Pn = As and Sb), Frandsen et al. reported the breaking of the 4-fold symmetry at low temperature without any superstructure peaks by neutron and electron diffractions[23] and suggested the possibility of intra-unit-cell nematic CDW, which is observed in cuprates and iron arsenides superconductors,[24−26] to account for the breaking. A theoretical suggestion was made that such an exotic CDW could be realized by the orbital ordering mediated by spin fluctuations.[27] Thus, the mechanism of structural transition in layered titanium-oxypnictides is still under debate.

Davies et al.[28] have just synthesized large single crystals of $Na_2Ti_2Pn_2O$ (Pn = As and Sb; Figure 1) in order to achieve reliable diffraction measurements and observed clear superstructure peaks of 2 × 2 × 2 and 2 × 2 × 1 for Pn = As and Sb, respectively. They did not detect any indication of spin orderings, so they concluded that the structural transition could be attributed to the conventional phonon-assisted CDW. From the theoretical side, examining whether or not the observed superstructures are explained by *ab initio* phonon calculations can provide a critical clue to the mechanism of structural transition. In the present study, we performed phonon

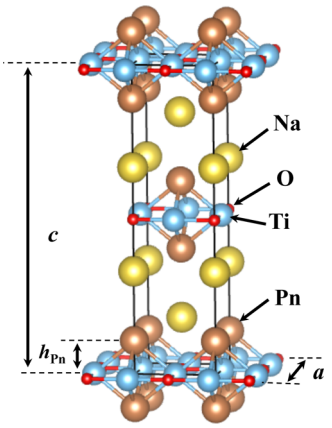

Figure 1. Crystal structure of $Na_2Ti_2Pn_2O$ (Pn = As and Sb). The space group is $I4/mmm$.

Received: July 9, 2017
Published: November 2, 2017

© 2017 American Chemical Society

DOI: 10.1021/acs.inorgchem.7b01709
Inorg. Chem. 2017, 56, 13732−13740

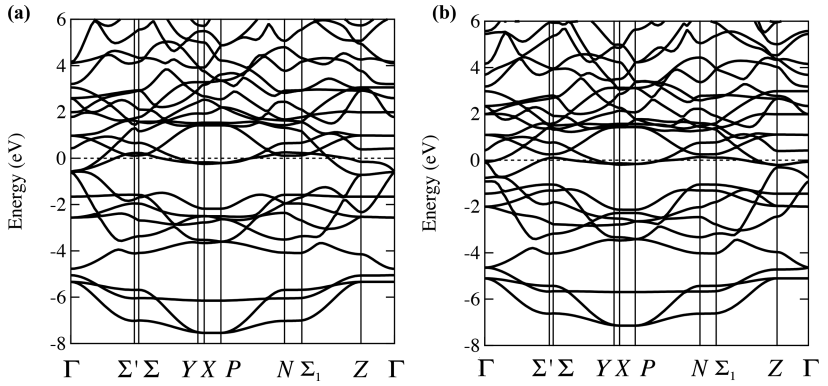

Figure 2. Electronic band structures for undistorted $Na_2Ti_2Pn_2O$ structure ((a) Pn = As, (b) Pn = Sb). The Fermi energy is set to 0 eV.

calculations for $Na_2Ti_2Pn_2O$ (Pn = As and Sb) using the GGA-PBE functional and compared the superstructures predicted by the calculations with the experimentally observed ones. The result shows that the phonon calculation can explain the observed *C*2/*m* (monoclinic No.12) structure for Pn = As, indicating that the present phonon calculation works well for this system. For Pn = Sb, however, we obtained a *Cmce* (orthorhombic No. 64) polymorph, being inconsistent with the observed one [*Cmcm* (orthorhombic No. 63)]. On the basis of these results combined with preceding studies[16,22,29−32] and further quantitative analysis, we propose a new possibility that a heavier Pn causes stronger electron correlations and induces the discrepancy.

RESULTS

Figure 2 shows band structures of undistorted $Na_2Ti_2Pn_2O$ (Pn = As and Sb). The results are consistent with the previous calculations,[32,33] meaning that there is no artifact due to the choice of cutoff, *k*-meshes, smearing parameters, and pseudo potentials. Figure 3a shows the phonon dispersions for Pn = As, giving imaginary frequencies appearing around $N = (2\pi/a)\cdot(1/2, 0, a/2c)$ and $\Sigma' = (2\pi/a)\cdot(1/2, 0, 0)$, where *a* and *c* are conventional lattice constants for the undistorted structure. The compatible modes with the experimental observation[28] where the twice larger periodicity along *c*-axis is realized are $N = (2\pi/a)\cdot(1/2, 0, a/2c)$ and $N' = (2\pi/a)\cdot(0, 1/2, a/2c)$. We note that the previous phonon calculation[34] could not reproduce this doubled periodicity. We therefore took these for further lattice relaxations from the original *I*4/*mmm* structure along the mode displacements to get the *C*2/*m* (monoclinic, No. 12) superstructure (Figures 4a and 5a), being consistent with the experiments.[28] The results of geometry optimizations for the undistorted (*I*4/*mmm*) and distorted (*C*2/*m*) structures are shown in Tables 1 and 2. The resultant optimized geometry of the *C*2/*m* superstructure gives fairly good agreement with the experiments[28] within deviations at most 2.5%.[35] Although we could not confirm whether or not the negative modes disappear in the *C*2/*m* superstructure even at high-symmetry points because of intractable computational costs for the enlarged unit cell, it should be confirmed in the future.

For Pn = Sb, we obtained phonon dispersions as shown in Figure 3b. Imaginary frequencies appear widely around $X = (2\pi/a)\cdot(1/2, 1/2, 0)$ and $P = (2\pi/a)\cdot(1/2, 1/2, a/2c)$. The experiment[28] reported that the twice larger super periodicity is realized only in *ab*-plane, not along *c*-axis. Therefore, the *X* mode is likely to realize the instability toward the superstructure. By optimizing the geometry along the mode

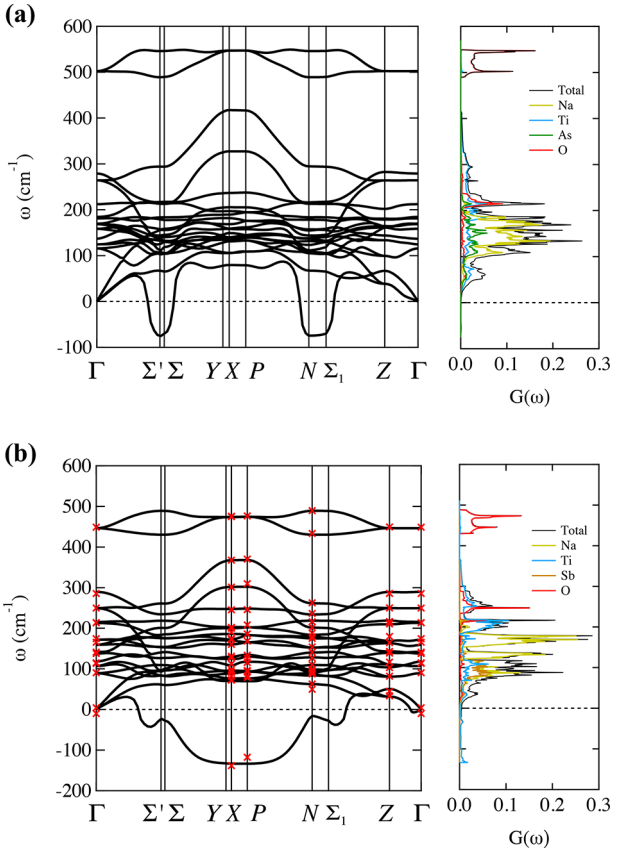

Figure 3. Phonon dispersions and phonon DOS for undistorted (*I*4/*mmm*) $Na_2Ti_2Pn_2O$ (Pn = (a) As, (b) Sb). The red cross marks in (b) represent the frequencies with spin−orbit coupling.

displacement, we obtained a *Cmce* (orthorhombic, No. 64, Figures 4b and 5b), being inconsistent with the observed *Cmcm* (orthorhombic, No. 63, Figure 4c) in the experiment.[28] To confirm the present conclusion further, we examined the stability by seeing if the imaginary frequencies disappear at the relaxed structure, as shown in Figure 6. In addition to the stability check, we compared enthalpies between our *Cmce* and the observed *Cmcm*. The optimized geometry with *Cmce* is found to be more stable by 1.1 (0.7) mRy per formula unit than that with *Cmcm* when using Marzari−Vanderbilt (Gaussian) smearing. These results indicate that the experimentally observed *Cmcm* is unfavorable at 0 K at the GGA level of DFT. It is, however, expected that GGA+*U* could reverse the order as discussed later. A comparison of Helmholtz free

DOI: 10.1021/acs.inorgchem.7b01709
Inorg. Chem. 2017, 56, 13732−13740

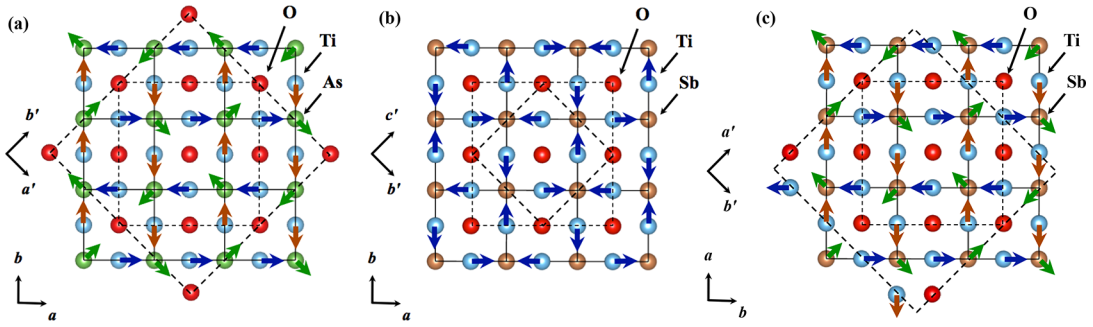

Figure 4. In-plane superstructures obtained by our calculations for Pn = (a) As and (b) Sb, and (c) the observed in-plane superstructure for Pn = Sb.[28] Pn is located above and below the Ti_2O plane. Solid lines represent the original unit cells for $I4/mmm$. Thin dash lines represent the unit cells for 2 × 2 superstructures. Solid dash lines represent redefined unit cells for distorted superstructures. The conventional lattice vectors of the superstructure for (a) Pn = As ($C2/m$) are redefined as $\vec{a'} = 2(\vec{a} - \vec{b})$, $\vec{b'} = 2(\vec{a} + \vec{b})$, and $\vec{c'} = 1/2(-\vec{a} + \vec{b} + \vec{c})$, those for (b) Pn = Sb ($Cmce$) are redefined as $\vec{a'} = \vec{c}$, $\vec{b'} = (\vec{a} - \vec{b})$, and $\vec{c'} = (\vec{a} + \vec{b})$, and those for (c) Pn = Sb ($Cmcm$) are redefined as $\vec{a'} = 2(\vec{a} + \vec{b})$, $\vec{b'} = 2(\vec{b} - \vec{a})$, and $\vec{c'} = \vec{c}$, where $\vec{a}$, $\vec{b}$, and $\vec{c}$ are conventional lattice vectors of the undistorted structures.

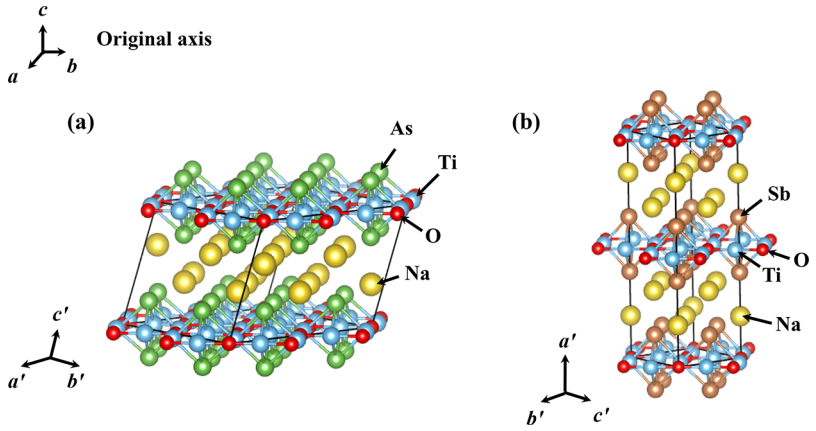

Figure 5. 3D superstructures obtained from our calculations for Pn = (a) As ($C2/m$) and (b) Sb ($Cmce$).

Table 1. Results of Geometry Optimization for Undistorted $Na_2Ti_2Pn_2O$ Structure (Pn = As and Sb)[a]

label	x	y	z	wyckoff
		Pn = As ($I4/mmm$)		
Na	0.50000	0.50000	0.18146	4e
Ti	0.50000	0.00000	0.00000	4c
As	0.00000	0.00000	0.11752	4e
O	0.50000	0.50000	0.00000	2b
		Pn = Sb ($I4/mmm$)		
Na	0.50000	0.50000	0.18369	4e
Ti	0.50000	0.00000	0.00000	4c
Sb	0.00000	0.00000	0.12015	4e
O	0.50000	0.50000	0.00000	2b

[a]The relaxed conventional lattice parameters are a = 4.07 Å, c = 15.44 Å (a = 4.14 Å, c = 16.98 Å) for Pn = As (Sb), giving good agreement with the experiments.[2,54] The height of Sb toward Ti_2O plane obtained from the present calculation is 2.04 Å, which is consistent with the experimental value at room temperature (2.01 Å).[54] For Pn = As, the height of As toward Ti_2O plane has not been determined in experiments, but the obtained value (1.81 Å) is quite consistent with the experimental results of $BaTi_2As_2O$ (1.77 Å)[4] and $(SrF)_2Ti_2As_2O$ (1.81 Å).[3]

Table 2. Results of Geometry Optimization for $Na_2Ti_2Pn_2O$ Superstructures (Pn = As and Sb) Obtained by Phonon Calculations[a]

label	x	y	z	wyckoff
		Pn = As ($C2/m$)		
Na	0.90907	0.00000	0.63699	4i
Na	0.40943	0.00000	0.63694	4i
Na	0.15932	0.24981	0.63725	8j
Ti	0.13031	0.11979	0.00000	8j
Ti	0.88019	0.36969	0.00000	8j
As	0.80877	0.00000	0.23625	4i
As	0.30933	0.00000	0.23625	4i
As	0.05905	0.24969	0.23623	8j
O	0.00000	0.00000	0.00000	2a
O	0.25000	0.25000	0.00000	4e
O	0.00000	0.50000	0.00000	2b
		Pn = Sb ($Cmce$)		
Na	0.18411	0.00000	0.00000	8d
Ti	0.00000	0.23266	0.26812	8f
Sb	0.37883	0.00000	0.00000	8d
O	0.00000	0.00000	0.00000	4a

[a]The conventional lattice parameters after relaxation are a'=11.51 Å, b' = 11.51 Å, c' = 8.23 Å, and β = 110.46° (a' = 17.04 Å, b' = 5.84 Å, and c' = 5.83 Å) for Pn = As (Sb).

energies ($E - TS$) under quasiharmonic approximation[36] is necessary to discuss the stability more precisely, where the entropic term is calculated from phonon DOS.[36] It was,

DOI: 10.1021/acs.inorgchem.7b01709
Inorg. Chem. 2017, 56, 13732−13740

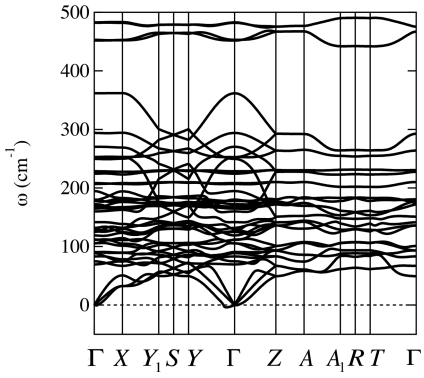

Figure 6. Phonon dispersions for $Na_2Ti_2Sb_2O$ superstructure (*Cmce*).

however, intractable because the large unit cell and the low symmetry of the *Cmcm* polymorph requires much more computational time to calculate its entropic term (*TS*). The results of geometry optimizations for the undistorted (*I*4/*mmm*) and distorted (*Cmce*) structures, and those for the experimentally observed superstructure (*Cmcm*) are shown in Tables 1−3.

Table 3. Results of Geometry Optimization for Experimentally Observed $Na_2Ti_2Sb_2O$ Superstructure[a]

label	*x*	*y*	*z*	wyckoff
		Pn = Sb (*Cmcm*)		
Na	0.00000	0.37498	0.93293	8f
Na	0.00000	0.12503	0.43294	8f
Na	0.74999	0.12500	0.93275	16h
Ti	0.37417	0.00083	0.25000	8g
Ti	0.62584	0.24918	0.25000	8g
Ti	0.87581	−0.00085	0.25000	8g
Ti	0.12418	0.25082	0.25000	8g
Sb	0.00000	0.37533	0.12909	8f
Sb	0.00000	0.12532	0.62908	8f
Sb	0.75033	0.12499	0.12907	16h
O	0.00000	0.62500	0.25000	4c
O	0.00000	0.12500	0.25000	4c
O	0.75000	0.37500	0.25000	8g

[a]The conventional lattice parameters after relaxation are a' = 11.74 Å, b' = 11.74 Å, and c' = 16.83 Å.

DISCUSSION

The present results confront the sharp contrast between Pn = As and Sb in terms of whether or not the present phonon calculations can reproduce the experimental structural phase transitions. Since it is clearly reported[28] that the measured XRD results cannot be identified by the $\sqrt{2} \times \sqrt{2} \times 1$ superstructure (Figure 4b), the discrepancy would be intrinsic so that it should be accounted for by the effects that are not taken into account in the present calculations. A spin−orbit effect is likely to be the origin of the discrepancy because Sb is heavier than As. To confirm, we again performed phonon calculations with fully relativistic pseudopotentials at high symmetry positions (Figure 3b). Although the frequencies slightly change because of the spin−orbit effect, the *X* point that induces the *Cmce* superstructure still shows the largest imaginary frequency. This result indicates that the spin−orbit effect is not the origin of the discrepancy.

We suggest the possibility that the GGA-PBE functional does not properly reproduce the electron correlation effects for Pn = Sb, and this could be the reason for the present discrepancy. The conclusion was obtained by the following discussion: In iron arsenide superconductors, the strength of electron correlation is well-captured by a trend of *h*, a vertical distance between Fe layer and Pn/Ch (Pn = P and As; Ch = Se and Te).[30] Miyake et al. applied constrained random-phase approximation (cRPA) to iron arsenide superconductors and revealed that the covalency of Fe-Pn/Ch bonding estimated by DFT-LDA calculation and the resultant Wannier orbitals can be used for a measure of the magnitude of electron correlation in the family.[30] When *h* gets larger, the covalency gets weaker to make Fe 3d more localized, and the spin/orbital polarizations get enhanced as one of the electron correlation effects. This measure probably works well for layered titanium-oxypnictides because they have crystal and electronic structures similar to those of iron arsenides.[8,15,23,30,31] In order to apply the measure to the layered titanium-oxypnictides, we quantitatively analyzed the covalencies of Ti−Pn bonding in $Na_2Ti_2Pn_2O$ (Pn = As and Sb). The ratio of partial density of states (pDOS) of each atom to total density of states (tDOS) can be used as a measure of covalency,[37,38] which is one of the common methods to evaluate covalency within DFT framework.[37−41] In this method, it is necessary to calculate a center of mass (CM) of atomic orbital for each atom. The CM is calculated by the following equation:[38]

$$\mathrm{CM}^{\mathrm{A}} = \frac{\int_{\varepsilon_2}^{\varepsilon_1} \varepsilon g^{\mathrm{A}}(\varepsilon)\, \mathrm{d}\varepsilon}{\int_{\varepsilon_2}^{\varepsilon_1} g^{\mathrm{A}}(\varepsilon)\, \mathrm{d}\varepsilon} \quad (1)$$

where A is an element, ε is an energy, $g^{\mathrm{A}}(\varepsilon)$ is pDOS of A at ε, and CM^{A} is a center of mass of the element A. Note that the energy window $[\varepsilon_2, \varepsilon_1]$ in the equation has to be chosen in such a way that it encompasses all relevant bands contributing to the bond.[38] The difference in CM can be used as a measure of covalency of the bond.[38] If the difference in the CM between X and Y ($|\mathrm{CM}^{\mathrm{X}} - \mathrm{CM}^{\mathrm{Y}}|$) is small, then the covalency of the bond is strong, and vice versa. Figure 7 shows the obtained pDOS and center of masses of Ti 3d, As 4p, and Sb 5p orbitals for $Na_2Ti_2Pn_2O$ (Pn = As and Sb). The pDOS indicates the existence of two types of bonds: One is Ti−O bonding contributing to [− 8.0 to −4.9 (4.5) eV], another is Ti−Pn bonding contributing to [− 4.9 (4.5) to 0.0 eV (Fermi energy)] for Pn = As (Sb). Note that the result that Ti−Pn bonding is related to Fermi surface is consistent with the previous study by Singh.[31] The lack of overlap between Pn and O states indicates that no Pn−O bonding is formed in the compound (Figure 7). Figure 7 shows that Ti−O bonding does not change between As and Sb. On the other hand, there is a significant difference in pDOS between As and Sb, indicating that the nature of Ti−Pn bonding changes between them. To quantify the covalencies of Ti−Pn bonding, we calculated the center of masses according to eq 1. The results are shown in Figure 7 as solid lines. We adopted $[\varepsilon_2, \varepsilon_1]$ = [− 4.9 eV, 0.0 eV] and [− 4.5 eV, 0.0 eV] for As and Sb, respectively. As a result, we obtained $|\mathrm{CM}^{\mathrm{Ti3d}} - \mathrm{CM}^{\mathrm{Sb5p}}|$ = 0.77 eV and $|\mathrm{CM}^{\mathrm{Ti3d}} - \mathrm{CM}^{\mathrm{As4p}}|$ = 0.68 eV. The smaller value of $|\mathrm{CM}^{\mathrm{Ti3d}} - \mathrm{CM}^{\mathrm{As4p}}|$ indicates that Ti−As bonding is more covalent than Ti−Sb bonding. According to electronegativity, which is one of the simplest measures of covalency, Ti−Sb bonding seems more covalent than Ti−As one. Our results, however, show that the simple measure is

DOI: 10.1021/acs.inorgchem.7b01709
Inorg. Chem. 2017, 56, 13732−13740

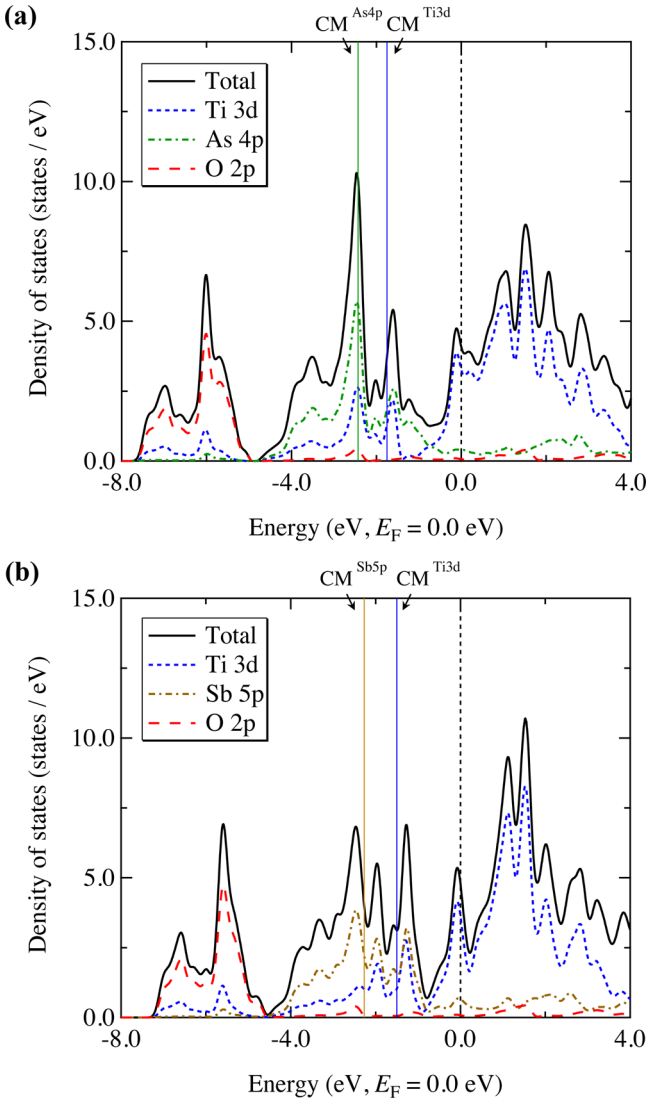

Figure 7. Partial density of states and center of masses of $Na_2Ti_2Pn_2O$ (a) Pn = As, (b) Pn = Sb.

invalid for the layered titanium-oxypnicitdes. In the compounds, the distance of Ti−Pn (the height of Pn toward Ti_2O plane) governs the covalency as well as electronegativity. This is the same trend as in iron arsenide superconductors. To confirm our conclusion, we also calculated electron density of $Na_2Ti_2Pn_2O$ and visualize (0 2 0) plane including Ti−Pn bondings. Figure 8 shows that the electron density between Ti−Sb (Ti−As) bonding is 0.03−0.04 electron/bohr^3 (0.04−0.05 electron/bohr^3). The result indicates that Ti−As bonding is more covalent than Ti−Sb one again, which is consistent with the above pDOS analysis. Our analysis implies the correlation effect gets more enhanced for Sb than As in layered titanium-oxypnictides. The trend is again consistent with our previous study for $BaTi_2Pn_2O$ (Pn = As, Sb, and Bi), where we showed that the phonon calculation using GGA-PBE could explain experiments only for Pn = As, but not for the other heavier Pn.[22] It might be a general tendency also applicable to the layered titanium-oxypnictides that the larger *h* enhances the electron correlation as the origin of the present discrepancy. Calculating the absolute values of electron correlation (e.g., effective Coulombic interaction, *U*) of the layered titanium-oxypnictides is an important future challenge.

Putting the discrepancy for Pn = Sb aside for a while, we can provide a plausible explanation for the origin of the lattice instability (Figure 3) from the above analysis: The lattice instability mainly derives from in-plane Ti displacements (Figure 4). To account for the interatomic forces to restore the lattice displacements, we can ignore (at least for the discussion of the instability) the contribution from Na because there are no bonds between Na and Ti (Figure 1). Starting with *X* mode for Pn = As and Sb, the imaginary frequency appears only for Pn = Sb. Figure 9a shows the change in potential energy accompanying the displacement of Ti atoms according to the phonon showing the imaginary (lowest) frequency at *X* point in Pn = Sb (As). The result shows that the original position is the most stable for Pn = As, but it is not for Pn = Sb. A double-well potential is realized for Pn = Sb. These phonons correspond to the Ti displacement toward Pn on the Ti_2O plane as shown in Figure 9b. One of possible restoring forces would come from the Coulombic attraction from the valence electrons between Ti and O atoms, but the force is almost

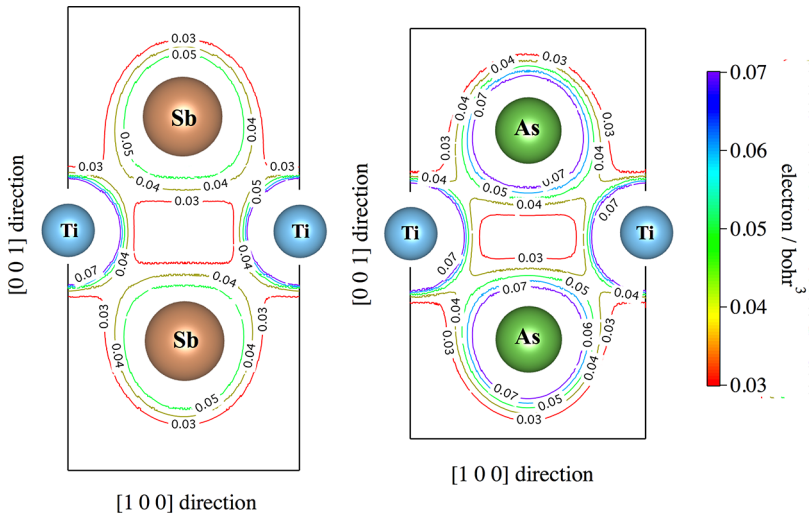

Figure 8. Electron densities of $Na_2Ti_2Pn_2O$ (a) Pn = As, (b) Pn = Sb along Ti−Pn bonds. The electron densities are plotted in the same range (0.03−0.07 electron/bohr^3), and the aspects are consistent with each crystal structure.

DOI: 10.1021/acs.inorgchem.7b01709
Inorg. Chem. 2017, 56, 13732−13740

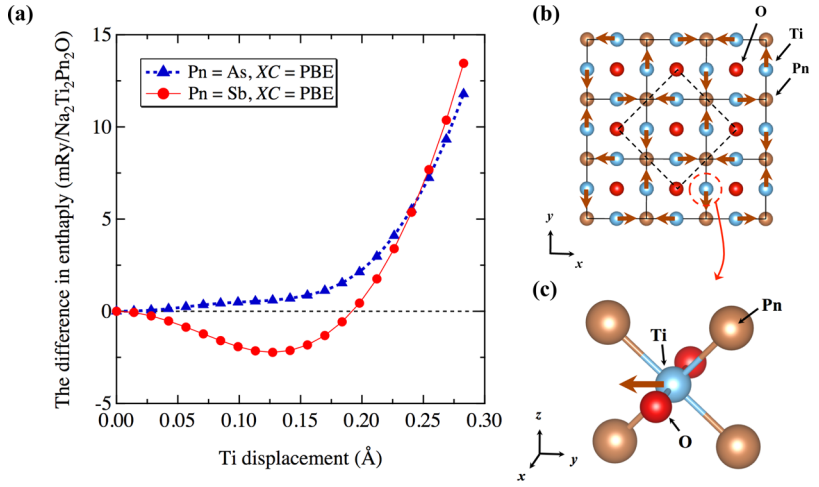

Figure 9. (a) Change in potential energy accompanying the displacement of Ti atoms according to the phonon showing the imaginary (lowest) frequency at *X* point in Pn = Sb (As). The horizontal axis corresponds to the magnitude of the displacement from the original positon. (b) Two-dimensional image of the displacement parttern of Ti atoms. (c) Three-dimensional image of the displacement parttern of the Ti atom enclosed in a red broken line in (b).

orthogonal to the displacement and hence we can ignore it.[42] In contrast, Pn is located in the same direction of Ti displacement, being responsible for the restoring forces. The displacement heads for the intermediate point of Pn located above and below the Ti_2O plane (Figure 9c). Ti atom is surrounded by these Pn (Figure 9c), so forces in the *z* direction were canceled. However, the forces in the *y* direction could be responsible for the restoring forces (Figure 9c). To discuss the difference between As and Sb, we focus on the high electron density region surrounded by Ti and Pn atoms (Figure 8). When we focus on the Ti atom shown in Figure 9c, it approaches (recedes from) the left (right) high electron density region. The Ti atom feels the Coulombic repulsion from the left region, because another Ti atom on the opposite side simultaneously approaches the region (Figure 9b). They compress the high electron density region, resulting in the increase of the Coulomb energy. The magnitude of the high density region is 0.04 electron/bohr^3 (0.03 electron/bohr^3) for Pn = As (Sb). This implies that the Coulombic repulsion effect in Pn = As is larger than that in Pn = Sb. In contrast, the Ti atom feels Coulombic attraction from the right region. The effect of Coulombic attraction is again larger for Pn = As because of the higher electron density of the region. These are the reasons for the difference that the original position is the most stable for Pn = As, but it is not for Pn = Sb. For *N* mode, the imaginary frequency appears commonly for Pn = As and Sb. This is also accountable along the above Discussion section. In this mode, the Ti−Pn interaction has little effect on the restoring forces because Ti and Pn move in the same direction (Figure 4a). The magnitude of the Coulombic repulsion and attraction from the high electron density region are expected to be much smaller because Pn moves in the same direction of Ti. In this case, the possible restoring force would originate from the nearest oxygen; again, this is orthogonal to the displacement, giving too weak a contribution and leading to the instability. This is the reason why the imaginary frequencies appear at *N* mode for both Pn.

We return to the discussion of the discrepancy for Pn = Sb. If the discrepancy is attributed to the electron correlation as we suggest, then calculations using exchange-correlation functionals beyond GGA such as GGA+*U* and hybrid functionals are necessary to reproduce the experimentally observed superstructure of Pn = Sb within DFT framework. Though we could not perform further phonon calculations with GGA +*U* or hybrid functional due to the limitation of the implementation, we note that an interesting case has been reported for $BaTi_2Sb_2O$ that only structural optimization with GGA+*U* could reproduce the observed transition from *P*4/*mmm* to *Pmmm*, otherwise without +*U* it cannot be explained.[43] GGA+*U* has also been applied to $Na_2Ti_2Sb_2O$[32] to examine possible magnetic orderings, identifying a bicollinear antiferromagnetic ordering is the most stable. The ordering is unfortunately not able to solely account for the observed superstructure,[28] but when combined with a phonon evaluation under the supposed ordering, it might give further instability toward the enlarged superstructure, which is possibly consistent with the observed symmetry. A model Hamiltonian can be used to explicitly take the electron correlation effect into consideration. In fact, plausible explanations for the observed intra-unit-cell nematic CDW transition,[23] which could not be explained by the present phonon calculations, have been proposed by using a model Hamiltonian.[27,43] The ideas are based on spin fluctuations to form magnetic orderings at low temperature, triggering another structural instability over the conventional prediction. Such a mechanism is not able to be described within the present calculation,[16,22] and could be a possible origin for the discrepancy. For the key issue (i.e. spin fluctuations), there are still a small number of experiments (NMR and μSR) giving the controversy about the existence of the fluctuations.[17−19,28,44] Inelastic magnetic neutron scattering can be expected to provide conclusive information about this.

CONCLUSIONS

We applied *ab initio* phonon analysis to layered titanium-oxypnictides, $Na_2Ti_2Pn_2O$ (Pn = As and Sb), and found a clear contrast between the cases with lighter/heavier pnictogen in comparison with experiments. The result completely explains the experimental structure at low temperature, *C*2/*m* for Pn = As, within the conventional charge density wave, while the calculation predicts that a *Cmce* polymorph is more stable than the experimentally observed superstructure (*Cmcm*) for Pn = Sb. To reveal the origin of discrepancy, we focus on the height

DOI: 10.1021/acs.inorgchem.7b01709
Inorg. Chem. 2017, 56, 13732−13740

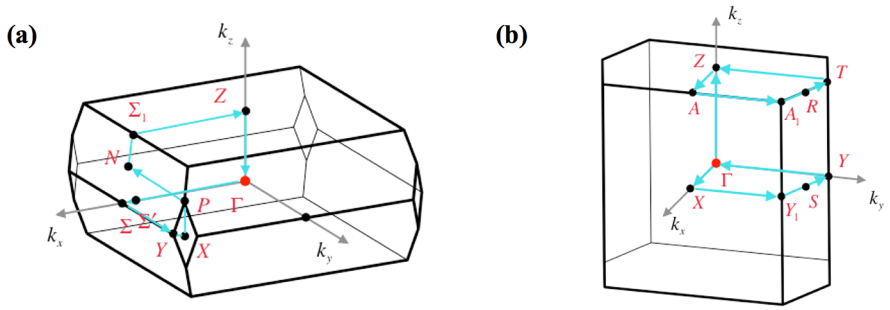

Figure 10. Primitive Brillouin zones (a) for undistorted $Na_2Ti_2Pn_2O$ structure (*I*4/*mmm*) and (b) for $Na_2Ti_2Sb_2O$ superstructure (*Cmce*).

of Pn toward Ti_2O plane in layered titanium-oxypnictides. This is because the strength of electron correlation is well-captured by a trend of *h*, a vertical distance between Fe layer and Pn or *Ch* in iron arsenide superconductors that have similar electronic structures to our layered titanium-oxypnictides. On the basis of quantitative analysis, we concluded that Ti−As bonding is more covalent than Ti−Sb one and the distance of Ti−Pn (the height of Pn toward Ti_2O plane) governs the covalency. The result indicates that the covalency of Ti−Pn bonding cannot be explained only by electronegativity in layered titanium-oxpnictides, which is the same trend as in iron arsenide superconductors. The result supports the similarity between iron arsenide and layered titanium-oxypnictide superconductors that has been proposed so far and probably stimulates further experimental and theoretical studies of layered titanium-oxypnictides. Our analysis could support the correlation effect gets more enhanced for Sb than for As in layered titanium-oxypnictides. Thus, we suggest the possibility that the GGA-PBE functional does not properly reproduce the electron correlation effects for Pn = Sb. This could cause the present discrepancy. If the discrepancy is attributed to the electron correlation as we suggest, then calculations using exchange-correlation functionals beyond GGA such as GGA+*U* and hybrid functionals are necessary to reproduce the experimentally observed superstructure of Pn = Sb. As shown in the present study, examining whether or not the observed superstructures are explained by *ab initio* phonon calculations can provide a clue to the mechanism of structural transition. The combination of diffraction studies and phonon calculations will be more important in the field of inorganic chemistry.

COMPUTATIONAL DETAILS

All the calculations were done within DFT using the GGA-PBE exchange-correlation functional,[45] implemented in Quantum Espresso package.[46] We chose the PBE functional because it has been used for the layered titanium-oxypnictides so for and then no critical discrepancy has been reported, for example, compared to the ARPES measurement.[21] We adopted PAW[47] pseudopotentials in most calculations. The present PAW implementation takes into account the scalar relativistic effects.[48,49] Only for spin−orbit case, we adopted Ultrasoft (US) pseudo potentials that take into account the fully relativistic effects.[48,49] We restricted ourselves to spin unpolarized calculations. The valence electron configurations used for the US and PAW pseudopotentials are $2s^22p^63s^1$ (Na), $3s^23p^63d^24s^2$ (Ti), $4s^24p^3$ (As), $5s^25p^3$ (Sb), and $2s^22p^4$ (O). Lattice instabilities were detected by the negative (imaginary) phonon dispersions evaluated for undistorted and distorted structures. Taking each of the negative phonon modes, the structural relaxations along the mode were evaluated by the BFGS optimization scheme with the structural symmetries fixed to *C*2/*m* for $Na_2Ti_2As_2O$ and *Cmce* for $Na_2Ti_2Sb_2O$. For phonon calculations, we used the linear response theory implemented in Quantum Espresso package.[50] Crystal structures and Fermi surfaces were depicted by using VESTA[51] and XCrySDen,[52] respectively.

To deal with all the compounds systematically, we checked the convergence of plane-wave cutoff energies (E_{cut}), *k*-meshes, *q*-meshes, and smearing parameters. The most strict condition among the compounds was taken to achieve the convergence within ±1.0 mRy per formula unit in the ground state energy, resulting in $E_{cut}^{(WF)}$ = 90 Ry for wave function and $E_{cut}^{(\rho)}$ = 800 Ry for charge density. For undistorted $Na_2Ti_2As_2O$ and $Na_2Ti_2Sb_2O$, (6 × 6 × 6) *k*-meshes were used for the Brillouin zone integration. Phonon dispersions were calculated on (6 × 6 × 6) *q*-meshes. For $Na_2Ti_2As_2O$ (*C*2/*m*) and $Na_2Ti_2Sb_2O$ (*Cmce*), (4 × 4 × 4) *k*-meshes were used. For $Na_2Ti_2Sb_2O$, (4 × 4 × 4) *q*-meshes were used to calculate phonon dispersions. We also calculated a ground state energy of the experimentally observed superstructure for $Na_2Ti_2Sb_2O$ (*Cmcm*)[28] with (6 × 6 × 3) *k*-meshes. The Marzari−Vanderbilt cold smearing scheme[53] with a broadening width of 0.01 Ry was applied to all the compounds. All the calculations were performed with primitive Brillouin zones.

The primitive Brillouin zone for undistorted $Na_2Ti_2Pn_2O$ (*I*4/*mmm*) is shown in Figure 10a. The special *k* and *q* points are Γ = $(2\pi/a)\cdot(0, 0, 0)$, *N* = $(2\pi/a)\cdot(1/2, 0, a/2c)$, *P* = $(2\pi/a)\cdot(1/2, 1/2, a/2c)$, *X* = $(2\pi/a)\cdot(1/2, 1/2, 0)$, Σ′ = $(2\pi/a)\cdot(1/2, 0, 0)$, and *Z* = $(2\pi/a)\cdot(0, 0, a/c)$ in Cartesian axis, where *a* and *c* are conventional lattice constants for the undistorted structures. The primitive Brillouin zone for $Na_2Ti_2Sb_2O$ superstructure (*Cmce*) is also shown in Figure 10b. The special *k* and *q* points are Γ = $(2\pi/a')\cdot(0, 0, 0)$, X = $(2\pi/a')\cdot(1, 0, 0)$, *S* = $(2\pi/a')\cdot(1/2, a'/2b', 0)$, *Z* = $(2\pi/a')\cdot(0, 0, a'/2c')$, *A* = $(2\pi/a')\cdot(1, 0, a'/2c')$, R = $(2\pi/a')\cdot(1/2, a'/2b', a'/2c')$ in Cartesian axis, where *a*′, *b*′, and *c*′ are conventional lattice constants for the superstructure.

AUTHOR INFORMATION

Corresponding Authors

*E-mail: kousuke_1123@icloud.com.
*E-mail: rmaezono@mac.com.

ORCID

Kousuke Nakano: 0000-0001-7756-4355
Kenta Hongo: 0000-0002-2580-0907

Notes

The authors declare no competing financial interest.

ACKNOWLEDGMENTS

The computation in this work has been performed using the facilities of the Research Center for Advanced Computing Infrastructure (RCACI) at JAIST. R.M. and K.H. are also grateful to MEXT-FLAGSHIP2020 (hp170269, hp170220) for their computational resources. K.H. is grateful for financial support from a KAKENHI grant (JP17K17762), a Grant-in-Aid for Scientific Research on Innovative Areas "Mixed Anion" project (JP16H06439) from MEXT, PRESTO (JPMJPR16NA) and the Materials research by Information Integration Initiative

DOI: 10.1021/acs.inorgchem.7b01709
Inorg. Chem. 2017, 56, 13732−13740

(MI²I) project of the Support Program for Starting Up Innovation Hub from Japan Science and Technology Agency (JST). R.M. is grateful to MEXT-KAKENHI (26287063, 17H05478), a Grant-in-Aid for Scientific Research on Innovative Areas "Mixed Anion" project (JP16H06440), a grant from the Asahi glass Foundation, and US-AFOSR-AOARD for their financial supports.

REFERENCES

(1) Axtell, E. A.; Ozawa, T.; Kauzlarich, S. M.; Singh, R. R. Phase Transition and Spin-gap Behavior in a Layered Tetragonal Pnictide Oxide. *J. Solid State Chem.* **1997**, *134*, 423.

(2) Ozawa, T. C.; Kauzlarich, S. M.; Bieringer, M.; Greedan, J. E. Possible Charge-Density-Wave/Spin-Density-Wave in the Layered PnictideOxides:$Na_2Ti_2Pn_2O$ (Pn = As, Sb). *Chem. Mater.* **2001**, *13*, 1804.

(3) Liu, R.; Song, Y.; Li, Q.; Ying, J.; Yan, Y.; He, Y.; Chen, X. Structure and Physical Properties of the Layered Pnictide-Oxides: $(SrF)_2Ti_2Pn_2O$ (Pn = As, Sb) and $(SmO)_2Ti_2Sb_2O$. *Chem. Mater.* **2010**, *22*, 1503.

(4) Wang, X. F.; Yan, Y. J.; Ying, J. J.; Li, Q. J.; Zhang, M.; Xu, N.; Chen, X. H. Structure and physical properties for a new layered pnictide-oxide: $BaTi_2As_2O$. *J. Phys.: Condens. Matter* **2010**, *22*, 075702.

(5) Doan, P.; Gooch, M.; Tang, Z.; Lorenz, B.; Moeller, A.; Tapp, J.; Chu, P. C. W.; Guloy, A. M. $Ba_{1-x}Na_xTi_2Sb_2O$ ($0.0 \le x \le 0.33$) A Layered Titanium-Based Pnictide Oxide Superconductor. *J. Am. Chem. Soc.* **2012**, *134*, 16520.

(6) Yajima, T.; Nakano, K.; Takeiri, F.; Ono, T.; Hosokoshi, Y.; Matsushita, Y.; Hester, J.; Kobayashi, Y.; Kageyama, H. Superconductivity in $BaTi_2Sb_2O$ with a d^1 Square Lattice. *J. Phys. Soc. Jpn.* **2012**, *81*, 103706.

(7) Yajima, T.; Nakano, K.; Takeiri, F.; Hester, J.; Yamamoto, T.; Kobayashi, Y.; Tsuji, N.; Kim, J.; Fujiwara, A.; Kageyama, H. Synthesis and Physical Properties of the New Oxybismuthides $BaTi_2Bi_2O$ and $(SrF)_2Ti_2Bi_2O$ with a d^1 Square Net. *J. Phys. Soc. Jpn.* **2013**, *82*, 013703.

(8) Yajima, T.; Nakano, K.; Takeiri, F.; Nozaki, Y.; Kobayashi, Y.; Kageyama, H. Two Superconducting Phases in the Isovalent Solid Solutions $BaTi_2Pn_2O$ (Pn = As, Sb, and Bi). *J. Phys. Soc. Jpn.* **2013**, *82*, 033705.

(9) Zhai, H.-F.; Jiao, W.-H.; Sun, Y.-L.; Bao, J.-K.; Jiang, H.; Yang, X.-J.; Tang, Z.-T.; Tao, Q.; Xu, X.-F.; Li, Y.-K.; Cao, C.; Dai, J.-H.; Xu, Z.-A.; Cao, G.-H. Superconductivity, charge- or spin-density wave, and metal-nonmetal transition in $BaTi_2(Sb_{1-x}Bi_x)_2O$. *Phys. Rev. B: Condens. Matter Mater. Phys.* **2013**, *87*, 100502.

(10) Nakano, K.; Yajima, T.; Takeiri, F.; Green, M. A.; Hester, J.; Kobayashi, Y.; Kageyama, H. T_c Enhancement by Aliovalent Anionic Substitution in Superconducting $BaTi_2(Sb_{1-x}Sn_x)_2O$. *J. Phys. Soc. Jpn.* **2013**, *82*, 074707.

(11) Pachmayr, U.; Johrendt, D. Superconductivity in $Ba_{1-x}K_xTi_2Sb_2O$ ($0 \le x \le 1$) controlled by the layer charge. *Solid State Sci.* **2014**, *28*, 31.

(12) von Rohr, F.; Nesper, R.; Schilling, A. Superconductivity in rubidium-substituted $Ba_{1-x}Rb_xTi_2Sb_2O$. *Phys. Rev. B: Condens. Matter Mater. Phys.* **2014**, *89*, 094505.

(13) Ji, Q.; Ma, Y.; Hu, K.; Gao, B.; Mu, G.; Li, W.; Hu, T.; Zhang, G.; Zhao, Q.; Zhang, H.; Huang, F.; Xie, X. Synthesis, Structural, and Transport Properties of Cr-Doped $BaTi_2As_2O$. *Inorg. Chem.* **2014**, *53*, 13089.

(14) Bednorz, J.; Müller, K. Possible high T_c superconductivity in the Ba-La-Cu-O system. *Z. Phys. B: Condens. Matter* **1986**, *64*, 189.

(15) Kamihara, Y.; Watanabe, T.; Hirano, M.; Hosono, H. Iron-Based Layered Superconductor $La[O_{1-x}F_x]FeAs$ (x = 0.05−0.12) with T_c = 26 K. *J. Am. Chem. Soc.* **2008**, *130*, 3296.

(16) Subedi, A. Electron-phonon superconductivity and charge density wave instability in the layered titanium-based pnictide $BaTi_2Sb_2O$. *Phys. Rev. B: Condens. Matter Mater. Phys.* **2013**, *87*, 054506.

(17) von Rohr, F.; Schilling, A.; Nesper, R.; Baines, C.; Bendele, M. Conventional superconductivity and charge-density-wave ordering in $Ba_{1-x}Na_xTi_2Sb_2O$. *Phys. Rev. B: Condens. Matter Mater. Phys.* **2013**, *88*, 140501.

(18) Kitagawa, S.; Ishida, K.; Nakano, K.; Yajima, T.; Kageyama, H. *s*-wave superconductivity in superconducting $BaTi_2Sb_2O$ revealed by $^{121/123}$Sb-NMR/nuclear quadrupole resonance measurements. *Phys. Rev. B: Condens. Matter Mater. Phys.* **2013**, *87*, 060510.

(19) Nozaki, Y.; Nakano, K.; Yajima, T.; Kageyama, H.; Frandsen, B.; Liu, L.; Cheung, S.; Goko, T.; Uemura, Y. J.; Munsie, T. S. J.; Medina, T.; Luke, G. M.; Munevar, J.; Nishio-Hamane, D.; Brown, C. M. Muon spin relaxation and electron/neutron diffraction studies of $BaTi_2(As_{1-x}Sb_x)_2O$: Absence of static magnetism and superlattice reflections. *Phys. Rev. B: Condens. Matter Mater. Phys.* **2013**, *88*, 214506.

(20) Gooch, M.; Doan, P.; Tang, Z.; Lorenz, B.; Guloy, A. M.; Chu, P. C. W. Weak coupling BCS-like superconductivity in the pnictide oxide $Ba_{1-x}Na_xTi_2Sb_2O$ (x = 0 and 0.15). *Phys. Rev. B: Condens. Matter Mater. Phys.* **2013**, *88*, 064510.

(21) Tan, S. Y.; Jiang, J.; Ye, Z. R.; Niu, X. H.; Song, Y.; Zhang, C. L.; Dai, P. C.; Xie, B. P.; Lai, X. C.; Feng, D. L. Photoemission study of the electronic structure and charge density waves of $Na_2Ti_2Sb_2O$. *Sci. Rep.* **2015**, *5*, 9515.

(22) Nakano, K.; Hongo, K.; Maezono, R. Phonon dispersions and Fermi surfaces nesting explaining the variety of charge ordering in titanium-oxypnictides superconductors. *Sci. Rep.* **2016**, *6*, 29661.

(23) Frandsen, B. A.; Bozin, E. S.; Hu, H.; Zhu, Y.; Nozaki, Y.; Kageyama, H.; Uemura, Y. J.; Yin, W.-G.; Billinge, S. J. L. Intra-unit-cell nematic charge order in the titanium-oxypnictide family of superconductors. *Nat. Commun.* **2014**, *5*, 5761.

(24) Lawler, M. J.; Fujita, K.; Lee, J.; Schmidt, A. R.; Kohsaka, Y.; Kim, C. K.; Eisaki, H.; Uchida, S.; Davis, J. C.; Sethna, J. P.; Kim, E.-A. Intra-unit-cell electronic nematicity of the high-T_c copper-oxide pseudogap states. *Nature* **2010**, *466*, 347.

(25) Kasahara, S.; Shi, H.; Hashimoto, K.; Tonegawa, S.; Mizukami, Y.; Shibauchi, T.; Sugimoto, K.; Fukuda, T.; Terashima, T.; Nevidomskyy, A. H.; Matsuda, Y. Electronic nematicity above the structural and superconducting transition in $BaFe_2(As_{1-x}P_x)_2$. *Nature* **2012**, *486*, 382.

(26) Fujita, K.; Hamidian, M. H.; Edkins, S. D.; Kim, C. K.; Kohsaka, Y.; Azuma, M.; Takano, M.; Takagi, H.; Eisaki, H.; Uchida, S.-i.; Allais, A.; Lawler, M. J.; Kim, E.-A.; Sachdev, S.; Davis, J. C. S. Direct phase-sensitive identification of a *d*-form factor density wave in underdoped cuprates. *Proc. Natl. Acad. Sci. U. S. A.* **2014**, *111*, E3026.

(27) Nakaoka, H.; Yamakawa, Y.; Kontani, H. Theoretical prediction of nematic orbital-ordered state in the Ti oxypnictide superconductor $BaTi_2(As, Sb)_2O$. *Phys. Rev. B: Condens. Matter Mater. Phys.* **2016**, *93*, 245122.

(28) Davies, N. R.; Johnson, R. D.; Princep, A. J.; Gannon, L. A.; Ma, J.-Z.; Qian, T.; Richard, P.; Li, H.; Shi, M.; Nowell, H.; et al. Coupled commensurate charge density wave and lattice distortion in $Na_2Ti_2Pn_2O$ (Pn = As, Sb) determined by X-ray diffraction and angle-resolved photoemission spectroscopy. *Phys. Rev. B: Condens. Matter Mater. Phys.* **2016**, *94*, 104515.

(29) Kuroki, K.; Usui, H.; Onari, S.; Arita, R.; Aoki, H. Pnictogen height as a possible switch between high-T_c nodeless and low-T_c nodal pairings in the iron-based superconductors. *Phys. Rev. B: Condens. Matter Mater. Phys.* **2009**, *79*, 224511.

(30) Miyake, T.; Nakamura, K.; Arita, R.; Imada, M. Comparison of *ab initio* low-energy models for LaFePO, LaFeAsO, $BaFe_2As_2$, LiFeAs, FeSe, and FeTe: electron correlation and covalency. *J. Phys. Soc. Jpn.* **2010**, *79*, 044705.

(31) Singh, D. J. Electronic structure, disconnected Fermi surfaces and antiferromagnetism in the layered pnictide superconductor $Na_xBa_{1-x}Ti_2Sb_2O$. *New J. Phys.* **2012**, *14*, 123003.

(32) Yan, X.-W.; Lu, Z.-Y. Layered pnictide-oxide $Na_2Ti_2Pn_2O$ (Pn = As, Sb): a candidate for spin density waves. *J. Phys.: Condens. Matter* **2013**, *25*, 365501.

DOI: 10.1021/acs.inorgchem.7b01709
Inorg. Chem. 2017, 56, 13732−13740

(33) Suetin, D.; Ivanovskii, A. Structural, electronic properties, and chemical bonding in quaternary layered titanium pnictide-oxides $Na_2Ti_2Pn_2O$ and $BaTi_2Pn_2O$ (Pn = As, Sb) from FLAPW-GGA calculations. *J. Alloys Compd.* **2013**, *564*, 117.
(34) Chen, D.; Zhang, T.-T.; Song, Z.-D.; Li, H.; Zhang, W.-L.; Qian, T.; Luo, J.-L.; Shi, Y.-G.; Fang, Z.; Richard, P.; Ding, H. New phase transition in $Na_2Ti_2As_2O$ revealed by Raman scattering. *Phys. Rev. B: Condens. Matter Mater. Phys.* **2016**, *93*, 140501.
(35) Note that we need to take special care when comparing our calculated geometry with an experimental one due to Davis et al.[28] We found that the atomic positions listed in their Table 1 are incompatible with their superstructure vectors, $\vec{a'} = 2(\vec{a} - \vec{b}), \vec{b'} = 2(\vec{b} - \vec{a})$, and $\vec{c'} = 1/2(\vec{a} + \vec{b} + \vec{c})$, described in their main text:[28] (1) If the description in the main text is assumed to be correct, then Na and Sb positions in the superstructure are respectively located unlikely far from their undistorted positions. (2) O is not located at (0.0, 0.0) in their Figure 6a, being inconsistent with their Table 1. Accordingly, we speculate that they again define the superstructure vectors compatible with the atomic positions in their Table 1, which differs from that in their main text. We also found $y = 0.0$ for As3 in their Table 1 must be a typo and correctly $y = 0.25$ because As3 should occupy 8j Wyckoff site and its undistorted position is $y = 0.5$. Assuming our speculation is correct, our optimized geometry parameters agree well with their experimental values.
(36) Van De Walle, A.; Ceder, G. The effect of lattice vibrations on substitutional alloy thermodynamics. *Rev. Mod. Phys.* **2002**, *74*, 11.
(37) Whangbo, M.-H.; Koo, H.-J.; Villesuzanne, A.; Pouchard, M. Effect of Metal-Oxygen Covalent Bonding on the Competition between Jahn-Teller Distortion and Charge Disproportionation in the Perovskites of High-Spin d^4 Metal Ions $LaMnO_3$ and $CaFeO_3$. *Inorg. Chem.* **2002**, *41*, 1920.
(38) Cammarata, A.; Rondinelli, J. M. Covalent dependence of octahedral rotations in orthorhombic perovskite oxides. *J. Chem. Phys.* **2014**, *141*, 114704.
(39) Hughbanks, T.; Hoffmann, R. Chains of trans-edge-sharing molybdenum octahedra: metal-metal bonding in extended systems. *J. Am. Chem. Soc.* **1983**, *105*, 3528.
(40) Dronskowski, R.; Bloechl, P. E. Crystal orbital Hamilton populations (COHP): energy-resolved visualization of chemical bonding in solids based on density-functional calculations. *J. Phys. Chem.* **1993**, *97*, 8617.
(41) Grechnev, A.; Ahuja, R.; Eriksson, O. Balanced crystal orbital overlap population—a tool for analysing chemical bonds in solids. *J. Phys.: Condens. Matter* **2003**, *15*, 7751.
(42) The angle of O−Ti−Pn becomes 87° even at the most stable point for Pn = Sb. The corresponding displacement is 0.125 Å (Figure 9a). In this case, the restoring force between Ti and the nearest O contributing to the direction of the displacement is negligible because cos(87°) is only 0.05.
(43) Zhang, G.; Glasbrenner, J. K.; Flint, R.; Mazin, I. I.; Fernandes, R. M. Double-stage nematic bond ordering above double stripe magnetism: Application to $BaTi_2Sb_2O$. *Phys. Rev. B: Condens. Matter Mater. Phys.* **2017**, *95*, 174402.
(44) Fan, G.; Zhang, X.; Shi, Y.; Luo, J. Charge density wave transition in $Na_2Ti_2Sb_2O$ probed by ^{23}Na NMR. *Sci. China: Phys., Mech. Astron.* **2013**, *56*, 2399.
(45) Perdew, J. P.; Burke, K.; Ernzerhof, M. Generalized Gradient Approximation Made Simple. *Phys. Rev. Lett.* **1996**, *77*, 3865.
(46) Giannozzi, P.; et al. QUANTUM ESPRESSO: a modular and open-source software project for quantum simulations of materials. *J. Phys.: Condens. Matter* **2009**, *21*, 395502.
(47) Blöchl, P. E. Projector augmented-wave method. *Phys. Rev. B: Condens. Matter Mater. Phys.* **1994**, *50*, 17953.
(48) Jollet, F.; Torrent, M.; Holzwarth, N. Generation of Projector Augmented-Wave atomic data: A 71 element validated table in the XML format. *Comput. Phys. Commun.* **2014**, *185*, 1246.
(49) Kucukbenli, E.; Monni, M.; Adetunji, B.; Ge, X.; Adebayo, G.; Marzari, N.; de Gironcoli, S.; Corso, A. D. Projector augmented-wave and all-electron calculations across the periodic table: a comparison of structural and energetic properties. **2014**, arXiv:cond-mat.mtrl-sci/1404.3015. *arXiv.org e-Print archive*. https://arxiv.org/abs/1404.3015 (accessed July 6, 2017).
(50) Baroni, S.; de Gironcoli, S.; Dal Corso, A.; Giannozzi, P. Phonons and related crystal properties from density-functional perturbation theory. *Rev. Mod. Phys.* **2001**, *73*, 515.
(51) Momma, K.; Izumi, F. VESTA3 for three-dimensional visualization of crystal, volumetric and morphology data. *J. Appl. Crystallogr.* **2011**, *44*, 1272.
(52) Kokalj, A. XCrySDen a new program for displaying crystalline structures and electron densities. *J. Mol. Graphics Modell.* **1999**, *17*, 176.
(53) Marzari, N.; Vanderbilt, D.; De Vita, A.; Payne, M. C. Thermal Contraction and Disordering of the Al(110) Surface. *Phys. Rev. Lett.* **1999**, *82*, 3296.
(54) Ozawa, T. C.; Pantoja, R.; Axtell, E. A.; Kauzlarich, S. M.; Greedan, J. E.; Bieringer, M.; Richardson, J. W. Powder Neutron Diffraction Studies of $Na_2Ti_2Sb_2O$ and Its Structure Property Relationships. *J. Solid State Chem.* **2000**, *153*, 275−281.

DOI: 10.1021/acs.inorgchem.7b01709
Inorg. Chem. 2017, 56, 13732−13740